PERGAMON

International Journal of Heat and Mass Transfer 45 (2002) 2289–2301

International Journal of HEAT and MASS TRANSFER

www.elsevier.com/locate/ijhmt

An integrated model for interaction between melt flow and non-equilibrium solidification in thermal spraying

X.Y. Wang [a], H. Zhang [b,*], L.L. Zheng [b], S. Sampath [a]

[a] *Department of Materials Science and Engineering, State University of New York at Stony Brook, Stony Brook, NY 11794-2275, USA*

[b] *Department of Mechanical Engineering, State University of New York at Stony Brook, Stony Brook, NY 11794-2300, USA*

Received 21 May 2001; received in revised form 16 October 2001

Abstract

In this paper, a micro/macro-integrated model based on the VOF scheme is presented that accounts for free surface movement, thermal contact resistance, and fluid instability. A sub-model is developed to include the non-equilibrium solidification phenomena at the solid/liquid interface. The melt flow is incorporated into the microscopic model through prescribing a velocity profile that is obtained from the interpolation of melt velocities on the macroscopic grids near the interface. To improve the efficiency of the integration between the melt flow and the microscopic model, a relational database is developed and applied to the integrated micro/macro model. Three velocity profiles, e.g., linear, parabolic, and cubic velocity profiles, are considered and the results are compared with those obtained from the diffusion model.

Keywords: Solidification; Materials processing; Spray; Micro/macro-integration model

1. Introduction

Thermal spray processes involve feed stock materials in powder or wire form injected into a high temperature jet, heated up and melted, and accelerated towards a substrate where a thin lamellae layer is formed after impingement, spreading, and solidification. Due to the complex physical changes taking place on a very short time scale, it is a difficult task to develop a good understanding of thermal spray processes, particularly the interaction between the free surface and evolution of the solidification interface.

Numerical simulation has been widely performed to simulate the free surface deformation and solidification. Several groups have employed the VOF-based computer packages such as SOLA-VOF, FLOW3D, RIPPLE [1] and their modified versions to study splat formation on a flat substrate. The dynamics of the free surface was captured by the VOF technique, and solidification was modeled through either applying a Stefan solution at the solidification interface or using the enthalpy method. The integration between the free surface deformation and rapid solidification has often been over-simplified. Trapage et al. [2,3] investigated the impact of a lead droplet in the absence of solidification using a three-dimensional code, FLOW-3D. By using a VOF-based computer package RIPPLE [1], Liu et al. [4,5] studied the splat formation and solidification processes. In particular, they studied the interaction between the free surface and solidification interface, and the interaction between two droplets impinging on a pre-determined non-flat surface [5,6]. Fukai et al. [7] and Zhao et al. [8] developed a model based on a deforming finite element method to study the deformation of a spherical liquid metal droplet impinging on a flat surface. They demonstrated the effects of the impact velocity, droplet diameter, surface tension, and materials properties on the fluid dynamics of the deforming droplet. Poulikakos and Waldvogel [9] investigated the

* Corresponding author. Tel.: +1-631-632-8492; fax: +1-631-632-8544.

E-mail address: hui.zhang@sunysb.edu (H. Zhang).

0017-9310/02/$ - see front matter
PII: S0017-9310(01)00328-3

Nomenclature

a	constant
Bi	Biot number, $Bi = hd/k$
C	constant
C_p	specific capacity (J kg^{-1} K^{-1})
d	thickness (m)
D	initial droplet diameter (m)
F	volume of fluid function
h	heat transfer coefficient (W m^{-2} K^{-1})
h_f	latent heat of fusion (J kg^{-1})
k	thermal conductivity (W m^{-1} K^{-1})
n	normal to interface
P	pressure (Pa)
Pr	Prandtal number, $Pr = v/\alpha$
Re	Reynolds number, $Re = \rho UD/\mu$
s	thickness of deposited layer (m)
St	Stefan number, $St = C_p(T_p - T_f)/h_f$
T	temperature (K)
T_p	initial droplet temperature (K)
t	time (s)
$\vec{u}$	velocity (m s^{-1})
U	impinging velocity (m s^{-1})
V_i	interface velocity (m s^{-1})
w	velocity component (m s^{-1})
We	Weber number, $We = \rho U^2 D/\sigma$

Greek symbols

α	thermal diffusivity (m s^{-2})
θ	non-dimensional temperature
μ	dynamic viscosity (N s m^{-2})
μ_k	linear kinetic coefficient (m s K^{-1})
δ	droplet thickness (m)
ρ	density (kg m^{-3})
σ	surface tension (N m^{-1})
Θ	volume fraction of fluid
κ	curvature (m^{-1})

Subscripts

c	Contact
f	fusion
i	interface
l	liquid
m	melting temperature
o	initial
p	impinging temperature
s	solid
sub	substrate
z	normal to interface

Superscripts

$*$	dimensional variable
–	dimensionless variable

droplet configuration and flow field at the onset of phase change, as well as the final solidified shape and revealed a strong coupling between the droplet dynamics and freezing behavior. Pasandideh-Fard et al. [10,11] simulated the impact and solidification of the tin droplets on a cold stainless steel substrate based on a modified SOLA-VOF method. Their results on the droplet shape matched well with the experimental data. Chung and Rangel [12] developed a numerical procedure for the simulation of metal droplet deposition processes with solidification, including undercooling and contact resistance, based on a one-dimensional approximation. Deplanque et. al. [13] developed a multidirectional solidification model in the RIPPLE code to investigate the micropore formation in solidifying molten metal droplets impinging on a cold substrate. Pasandideh-Fard et al. [14] conducted 3D impact and solidification simulations based on a 3D VOF model and the enthalpy method for solidification. Zheng and Zhang [15] developed a 3D model that utilized adaptive grid generation and adaptive level set formulation to study the droplet deformation and solidification simultaneously for a molten metal droplet impinging on a substrate and on an inclined surface of 45°. Zhang et al. [16] integrated a VOF-based fluid flow solver with rapid solidification model to study the splat formation and substrate melting. Though the non-equilibrium feature has been studied in some cases, the influences of melt convective on rapid solidification have been neglected [12,16–19].

In this paper, a micro/macro-integrated model is developed to study the droplet deformation, melt flow, and wall interaction during the splat formation, considering the effects of melt flow on rapid solidification. In the integrated model, the free surface location and movement are captured by the modified VOF technique [16], and the movement of solidification interface is determined by applying energy balance and the kinetic correlation between the interface velocity and temperature at the interface. The melt flow is incorporated into the microscopic model through prescribing a velocity profile that is obtained from the interpolation of melt velocities on the macroscopic grids near the interface. To improve the efficiency of the integration between the melt flow and the microscopic model, a relational database is developed and applied to the integrated micro/macro model. The effects of the droplet size, impact velocity, superheating of droplet, and substrate temperature on splat solidification for different velocity profiles are investigated. Interaction between a droplet and a pre-deposited splat is also investigated.

2. Mathematical models

In order to simulate the impinging, spreading, and solidification of a molten metal droplet on a cold substrate accurately, it is necessary to solve the full Navier–Stokes equations and to track both the free surface deformation and the solid/liquid interface. The model combines a VOF-based numerical solution of the Navier–Stoke equations and a multi-directional rapid solidification model that considers the kinetic correlation between the interface velocity and temperature.

2.1. Fluid flow and heat transfer

The enthalpy method has been widely used in the open literature for droplet solidification. By introducing the mass fraction of the solidified material, transport phenomena are described by one set of governing equations for the entire domain. The value of mass fraction is defined as zero and unity in the control volume containing the liquid and solid, respectively, and between zero and unity in the control volume containing the interface. The energy equation is written in terms of enthalpy. The continuum formulation for the entire region eliminates the need for tracking interfaces with an assumption of local thermal equilibrium. To study rapid solidification, local equilibrium approximation is no longer applicable. A different approach must be developed.

In this paper, we assume that the droplet melt behaves like a Newtonian fluid; the flow motion is two-dimensional, axi-symmetric, and laminar; thermophysical properties are invariant to temperature (without buoyancy force); changes in thermal conductivity and heat capacity due to phase change are included but the mass densities of the melt and its solid are the same (i.e., no volumetric change upon phase change). In consideration of these assumptions, the problem is described mathematically by the continuum conservation equations for mass, momentum, and energy as follows,

$$\nabla \cdot \vec{u} = 0, \tag{1}$$

$$\bar{\rho}\left(\frac{\partial \vec{u}}{\partial t} + \nabla \cdot (\vec{u}\vec{u})\right) = -\nabla \bar{P} + \frac{1}{Re}\nabla \cdot (\bar{\mu}\nabla \vec{u}) + \frac{\kappa}{We}\nabla F, \tag{2}$$

$$\bar{\rho}\bar{C}_{\mathrm{p}}\left(\frac{\partial \theta}{\partial t} + \nabla \cdot (\vec{u}\theta)\right) = \frac{1}{Re\,Pr}\nabla \cdot (\bar{k}\nabla \theta), \tag{3}$$

where $\bar{\rho}$, $\bar{C}_{\mathrm{p}}$, $\bar{\mu}$, and $\bar{k}$ are the non-dimensional density, specific heat, viscosity, and thermal conductivity, respectively. κ is the local curvature of the free surface. The governing equations (1)–(3) are non-dimensionalized using the following variables:

$$\begin{aligned} &(u, v) = (u^*, v^*)/U \quad t = t^* U/D, \\ &P = P^*/(\rho U^2), \quad \theta = (T - T_{\mathrm{f}})/(T_{\mathrm{p}} - T_{\mathrm{f}}). \end{aligned} \tag{4}$$

The last term in Eq. (2) represents the surface tension force concentrated at the free surface. The problem is characterized by the *Re*, *Pr*, and *We* numbers. Here we assume that a sharp interface exists between the molten droplet and the substrate/deposited layer. The thermophysical properties μ and k in the interface are evaluated as:

$$k = k_{\mathrm{l}}\Theta + k_{\mathrm{s}}(1 - \Theta), \quad \mu = \mu_{\mathrm{l}}/\Theta, \tag{5}$$

where Θ is the fractional volume of the fluid in the control volume containing the solid/melt interface. The value of the fractional volume can be obtained from the position of the solidification interface. The fractional volume of the fluid function, F, is defined as unity in any control volume fully occupied by fluid, zero in any control volume occupied by void, and between zero and unity in any control volume containing free surface. The transport equation of the VOF function F can be written as follows,

$$\frac{\partial \Theta F}{\partial t} + \nabla \cdot (\vec{u}\Theta F) = 0. \tag{6}$$

Eqs. (1)–(6) can be solved iteratively to obtain the melt flow, heat transfer, and free surface deformation with a given position of the solidification interface.

2.2. Rapid solidification

The distinguishing feature of rapid solidification in thermal spraying is the non-equilibrium phase transformation with a large melt undercooling and a high solidification rate. The importance of non-equilibrium kinetics in rapid solidification has stimulated extensive research and significant progress has been made in understanding of the transport phenomena underlying rapid solidification [16,19]. In the classical equilibrium solidification model, the interface is defined at the location where temperature is at the freezing point of the material. The rate of solidification is, thus, controlled by a heat flux balance at the interface. This treatment, however, does not include the undercooling phenomena, which is of great importance to rapid solidification processes during thermal spray coating. It is believed that substantial undercooling is present at the beginning of the freezing process, and it diminishes as solidification proceeds. To consider the kinetic effect during rapid solidification, a correlation between the undercooling and the rate of solidification is required. The linear relationship,

$$V_{\mathrm{i}} = \overline{\mu_{\mathrm{k}}}(\theta_{\mathrm{f}} - \theta_{\mathrm{i}}), \tag{7}$$

is used in this study. In Eq. (7), $\overline{\mu_{\mathrm{k}}}$ is the non-dimensional linear kinetics coefficient, and θ_{f} and θ_i are the

Table 1
Thermophysical properties used in the calculations

	Mo	Steel
T_m (K)	2883	1788
h_f (J kg^{-1})	3.71×10^5	2.72×10^5
k_l (W m^{-1} K^{-1})	46	26
k_s (W m^{-1} K^{-1})	84	28
C_{pl} (J kg^{-1} K^{-1})	570	866.67
C_{ps} (J kg^{-1} K^{-1})	339	690.82
ρ_l(kg m^{-3})	9350	7700
ρ_s(kg m^{-3})	10200	7850
α_l(m^2 s^{-1})	0.86×10^{-5}	0.39×10^{-5}
α_s (m^2 s^{-1})	2.43×10^{-5}	0.52×10^{-5}
μ_k (m s K^{-1})	0.26	0.01

equilibrium freezing temperature and actual interface temperature, respectively. The term, $\theta_f - \theta_i$, represents the undercooling.

The energy balance condition at the solidification interface is expressed as follows

$$\frac{\partial s}{\partial t} = \frac{St}{Re\,Pr}\left(\nabla\theta_l - \frac{k_s}{k_l}\nabla\theta_s\right)\cdot\nabla s \tag{8}$$

where $s(r,t)$ is the thickness of the solidified layer.

Due to an imperfect contact between the droplet and substrate, thermal contact resistance should be modeled. The boundary condition between the deposit and substrate can be written as

$$\frac{\partial\theta}{\partial n} = Bi_c(\theta_{p,i} - \theta_{sub,i}), \tag{9}$$

where $\theta_{p,i}$ and $\theta_{sub,i}$ are the droplet and substrate temperatures at the interface between the deposit and substrate, respectively. $Bi_c = h_c d/k_{sub}$ is the Biot number. For simplicity, a constant heat transfer coefficient $h_c = 5 \times 10^7$ W m^{-2} K^{-1} is used to quantify the contact resistance. It is noted that thermal contact resistance, in reality, is a function of impacting velocity, surface roughness, and wetting ability, and it changes during the processes. The substrate temperature far away from the deposit, θ_{sub}, is assumed to be constant. An adiabatic thermal condition is applied to the surface of the droplet and the top surface of the substrate, and the initial conditions are $\theta = \theta_p$ for the droplet and $\theta = \theta_{sub}$ for the substrate. Table 1 lists the thermophysical properties used in the simulation.

3. Numerical method

As we mentioned earlier, the enthalpy method assumes local thermal equilibrium. It is, therefore, not applicable in the region where rapid solidification occurs. To consider the thermal non-equilibrium, Eqs. (7) and (8) have to be used to determine the interface location, the rate of solidification, and the mass fraction of the liquid. A micro/macro-integrated scheme is developed here considering the effect of melt flow on rapid solidification. Fig. 1 shows the schematic of the integration scheme. Eqs. (1)–(3) and (6) are solved in the macroscopic level and the interface location and shape, and velocity distribution near the interface are the input for the microscopic model. The microscopic model is applied to the dark points (see Fig. 1), which are located at the center of the interface in each node. The microscopic model based on rapid solidification is therefore solved at each node containing the interface. The interface location in the microscopic level is tracked explicitly. The time step is much smaller in a microscopic model necessary to obtain a stable and accurate result. The length scale is also shorter since the melt undercooling only appears near the interface. During the microscopic calculation, the velocity fields remain unchanged within a macroscopic time step. The temperature distribution as well as the interface location is predicted. The new interface position is feed back to the macroscopic model and the new interface location at each dark point is determined. The new interface position and shape can then be reconstructured from those dark points. The governing equations are then solved again in the macroscopic level together with the new interface location. The procedure is repeated until the final time is reached. Several numerical issues are addressed briefly in the following.

Different time scales are employed in the microscopic and macroscopic models. The microscopic model is solved on a one-dimensional computational domain. A time step of 10^{-4} μs is usually used. The time step is determined from the grid independent studies. The time step used in the fluid flow simulation varies and is determined by the instability criteria of Kothe et al. [1]. The time-step for the melt flow simulation begins from 10^{-3} μs, and increases gradually to 0.1 μs. It finally maintains at 0.1 μs. The time scale used in the microscopic rapid solidification model is therefore much shorter than that used in the macroscopic fluid flow and heat transfer simulation. In each macroscopic time step, multiple microscopic time steps have been executed in the microscopic level.

The interaction between melt flow in the macroscopic level and rapid solidification in the microscopic level are considered by employing two sets of computational grids. The macroscopic governing equations are solved on a non-uniform mesh (200×60) for the entire computational domain including the deformable droplet, the solidified layer and the substrate. When the droplet impacts on a substrate, the energy equation along with the interface conditions (Eqs. 7 and 8) is solved in the vicinity of the solidification interface using 600 grids on each side to ensure rapid solidification resolved in the fine grids. The computational domain, interface loca-

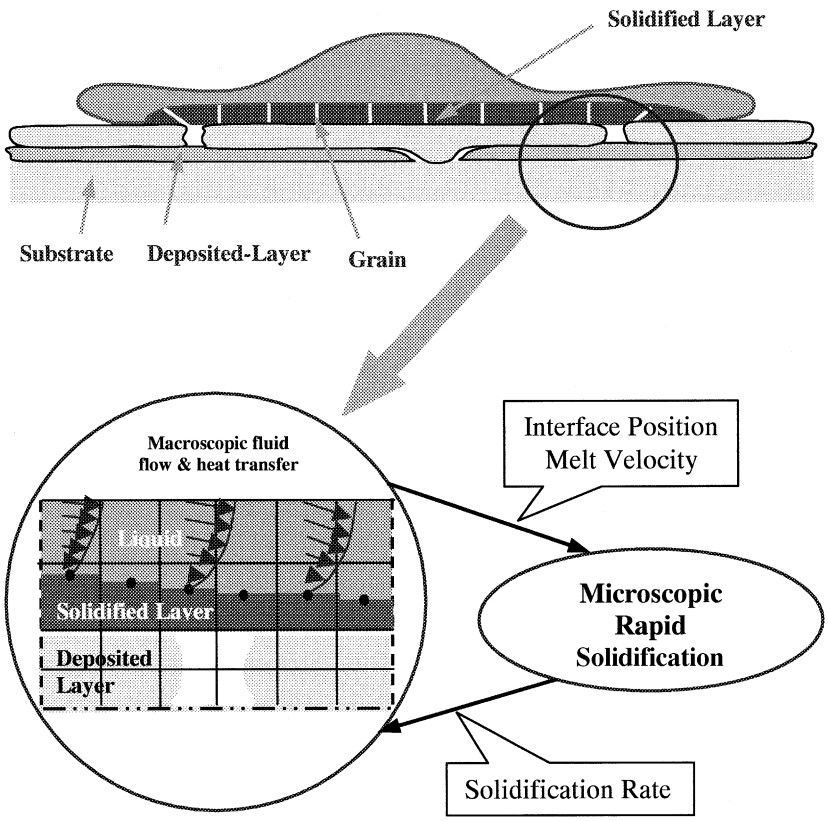

Fig. 1. Schematic of the integration method between macroscopic melt flow model and microscopic rapid solidification model.

tion, and grid size change in the microscopic solidification calculation. The grid size is much finer than that used in the macroscopic level. To consider the effect of melt flow on rapid solidification, the melt velocity distribution should be available at the finer grids. In this paper, we prescribe a velocity profile near the interface. If the droplet is assumed to remain a cylindrical disk shape during its deformation, the following three velocity profiles can be derived: (a) linear profile, $w_z = -Cz$, (b) parabolic profile, $w_z = -Cz^2$, and (c) cubic profile, $w_z = -Cz^2(z - 3\delta)$ [20], where, w_z is the velocity in the direction normal to the substrate, C is a constant coefficient, δ is the droplet thickness, and z is the normal direction to the substrate. The parameters, C and δ, of the velocity profile are obtained from the melt velocity on the coarse grids near the solid/liquid interface. The parabolic and cubic profiles proposed here can have zero value at the solidification interface, and they also preserve the mass conservation and maintain zero shear stress at the free surface [13,20]. From the mathematical point of the view, the cubic profile leads to the best prediction. The obtained velocity profile is then integrated into the transient energy equation in the microscopic model, in which the convection terms are included in the energy equation as source terms. The rapid solidification with melt flow is solved sequentially to obtain the solidification rate $\partial S/\partial t$. For a time increment of Δt, the movement of the solid/liquid interface in the direction normal to the interface at each grid is calculated as

$$\Delta S = \sum \frac{\partial S}{\partial t} \Delta t. \tag{10}$$

Since the time step used in the macroscopic fluid flow solver is much larger, the total increase of the solidified thickness in a macroscopic time step is a summation of the thickness increment in every microscopic time step. A numerical integration, the Trapezoidal rule, is employed to improve the accuracy of the summation. The shape and location of the coating layer are updated afterwards. The volume fraction of the liquid, Θ, and the thermophysical properties are updated subsequently using Eq. (5), and the calculation at the macroscopic level is executed again until the convergent results are achieved.

The microscopic solidification model is exercised on each macroscopic grid containing the solidification interface. The same calculation is repeated for every macroscopic time step. It is an expensive process since the total time step and the grid number required to

obtain an accurate result are very large. To speed up the calculation, a database technology is used. It is easy to understand that the solidification rate is the most important information needed for the macroscopic model. It is used to update the interface location and the mass fraction. The solidification rate depends on temperature boundary conditions and velocity profiles in the microscopic level. In the new scheme, one-dimensional rapid solidification is calculated first for different boundary conditions with a prescribed velocity profile. The rate of solidification versus time is recorded and saved in a tabulated form as a database. Three databases are generated for three velocity profiles with given boundary conditions. After comprehensive databases are generated, the macroscopic fluid flow solver is executed. The melt flow field and temperature distribution are solved. The boundary conditions and velocity profile for the microscopic model are obtained. The rate of solidification is obtained from querying data from the lookup tables. The numerical integration of Eq. (10) is applied to obtain the interface movement at each interface grid. It should be pointed out that we only deal with a droplet impinging on a substrate with a high conductivity, and the cooling rate is dominant in the vertical direction. Two-dimensional effects are, therefore, not significant. All computations are performed on a DELL Dimension XPS R450 PC. Each macroscopic simulation takes about 40 min CPU time using a 200×60 mesh. Note that a significant amount of computation time (several days) is needed to run the cases for constructing database.

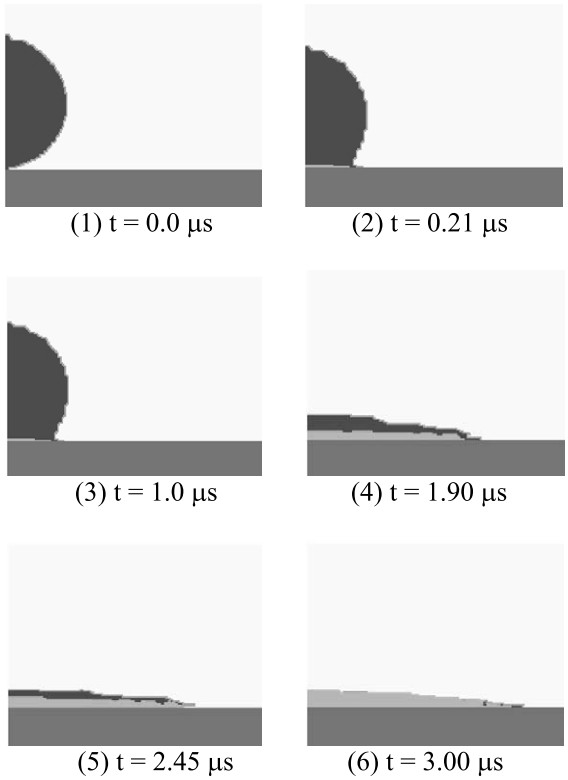

Fig. 2. Free surface evolution and solidification at different time when a molybdenum droplet of 50 μm diamter and 2983 K impinges on a stainless steel substrate of 400 K at 50 m/s.

4. Results and discussion

A two-dimensional model is applied to simulate a molybdenum droplet impinging and solidifying on a stainless steel substrate. The baseline case representing actual spray deposition processes is defined as follows: $D = 50$ μm, $U = 50$ m/s, $T_p = 2983$ K, and $T_{sub} = 400$ K. A 200×60 non-uniform grid is used in the macroscopic simulation of melt flow and heat transfer. Fig. 2 shows the free surface and interface location at different times for the baseline case. In the simulation, the effect of melt convection on rapid solidification is considered and a second-order polynomial velocity profile is used in the solidification model. The droplet begins to solidify at about $t = 0.2$ μs, and a disk-like splat is obtained at $t = 3.0$ μs. The Reynolds number of the droplet is 3686, and the flattening ratio of the splat is 3.42. The flattening ratio is defined as the ratio of the maximum diameter of the spreading splat to the initial droplet diameter. The ratio of splat–flattening ratio to $Re^{0.2}$ is 0.66. The analytical solution of the splat–flattening ratio shows that the ratio of splat–flattening ratio to $Re^{0.2}$ should be about unity or less depending on the solidification rate [16,21]. The results in Fig. 2 are similar to those obtained using the enthalpy method for splat solidification. However, very different solidification rates at the beginning of the process are obtained from the simulations using a non-equilibrium or an equilibrium solidification model. Since the microstructure of the splat is based on the initial rate of solidification, a finer grain will be obtained if the solidification rate is higher. The morphology and instability of the splat may also be determined by the initial rate of solidification. The undercooling temperature, however, diminishes very fast and equilibrium solidification occurs at the later stage of the process. The final shape of the splat is therefore similar to that predicted by the enthalpy method.

It is important to understand rapid solidification and the effects of melt flow on the solidification rate. In this paper, the effects of droplet size, initial substrate temperature, initial droplet temperature, and impinging velocity on the rate of solidification will be investigated. Since the rate of solidification varies along the solid/liquid interface, variations of the solidification thickness at the central location of the droplet with time are plotted and the results are compared with those obtained using the diffusion model.

4.1. Effect of velocity profile

Numerical simulations are performed to investigate the effects of different velocity profiles on rapid solidification. Three velocity profiles, linear, parabolic, and cubic, are used together with the diffusion case (without considering melt convection in rapid solidification). Fig. 3 shows the thickness of the solidified layer at the center location of the splat as a function of time for the baseline case for four different velocity profiles (zero, linear, parabolic, and cubic). It is evident that very different results are obtained between those obtained from a linear profile and solidification without considering melt flow. This is easy to explain since the melt flow will enhance heat transfer in the melt, and the solidification rate decreases when the melt flow is included. The velocity profiles are important in accurate prediction of the solidification rate. The linear profile exhibits the slowest solidification rate among three profiles. The results from the parabolic profile are somewhere in between. At the beginning of the process, the result from the parabolic profile is close to that using the linear profile, and at the end of the process, the result deviates to that of the diffusion case. The result obtained from the cubic profile resides somewhere between those from the linear and parabolic profiles. It is concluded that the results from the diffusion model overestimate the rate of solidification, while the results using the linear profile underestimate the rate. Theoretically, the second- and third-order velocity distributions will be more close to reality.

4.2. Effect of droplet size

The experimental data for thermal spraying indicate that transport phenomena obtained from a small droplet size with a high impact velocity is quite different from that obtained from a large droplet with a low impact velocity. It is believed that the surface tension, the interaction between the droplet and substrate, surface roughness, and rapid solidification all play significant roles [16]. In this paper, we limit our attention to the effects of melt flow on rapid solidification in the microscopic model, and the interaction between the droplet and substrate in the macroscopic model. The surface roughness is neglected. Numerical study is undertaken to investigate the role of the droplet size on rapid solidification considering melt flow. To clarify whether the droplet size plays an important role in solidification during a molybdenum droplet impact on a stainless steel substrate, three different droplet sizes, $D = 10$, 30, and 50 μm, are used and three different velocity profiles are considered. Figs. 4(a)–(d) show the effects of melt flow on solidification rates for different sizes of the droplet. It is clear that melt flow does not play an important role for a small droplet (diameter less than 10 μm), but it does for a large droplet (diameter greater than 50 μm). Heat loss on the substrate becomes a dominating mode for a smaller droplet, and heat transfer in the molten liquid is less significant. It is, however, crucial to consider the velocity profile correctly in the melt for a larger droplet. We conclude that, for the impacting velocity of 50 m/s, the melt flow is not important for a droplet size of less than 30 μm, while the melt convection is important in determining the solidification rate for a droplet size of greater than 30 μm.

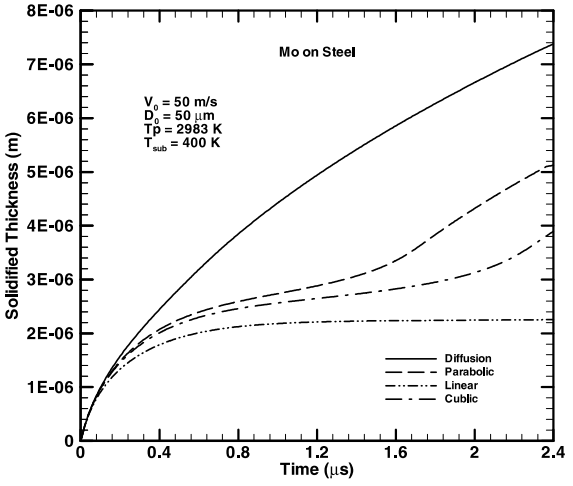

Fig. 3. The solidified thickness as a function of time for $D = 50$ μm, $U = 50$ m/s, $T_{in} = 2983$ K, and $T_{sub} = 400$ K during a molybdenum droplet impacting on a stainless steel substrate.

4.3. Effect of substrate temperature

In addition to the thermophysical properties of the substrate, its initial temperature affects the interface velocity significantly [22]. In experiments, the substrate is often heated up before spraying to improve the wetting ability of the surface. It is therefore important to consider the effect of melt flow on the solidification rate for different initial substrate temperatures. Fig. 3 shows the effect of different velocity profiles on solidification for $T_{sub} = 400$ K. To demonstrate the influence of the initial substrate temperature on the solidification rate, three substrate temperatures, $T_{sub} = 300$, 400, 500 K, are employed. As shown in Figs. 5(a)–(d), under different velocity profiles, an increase of the initial substrate temperature leads to a slight decrease of the solidification rate, in particular for the linear and diffusion cases. At the earlier stage of solidification, initial substrate temperature has virtually no effect on the solidification rate. Nevertheless, this conclusion may not be extended to other materials. The equilibrium freezing temperature of molybdenum is much higher than the substrate temperature. Further increasing of the initial substrate temperature is not possible due to the oxidation of

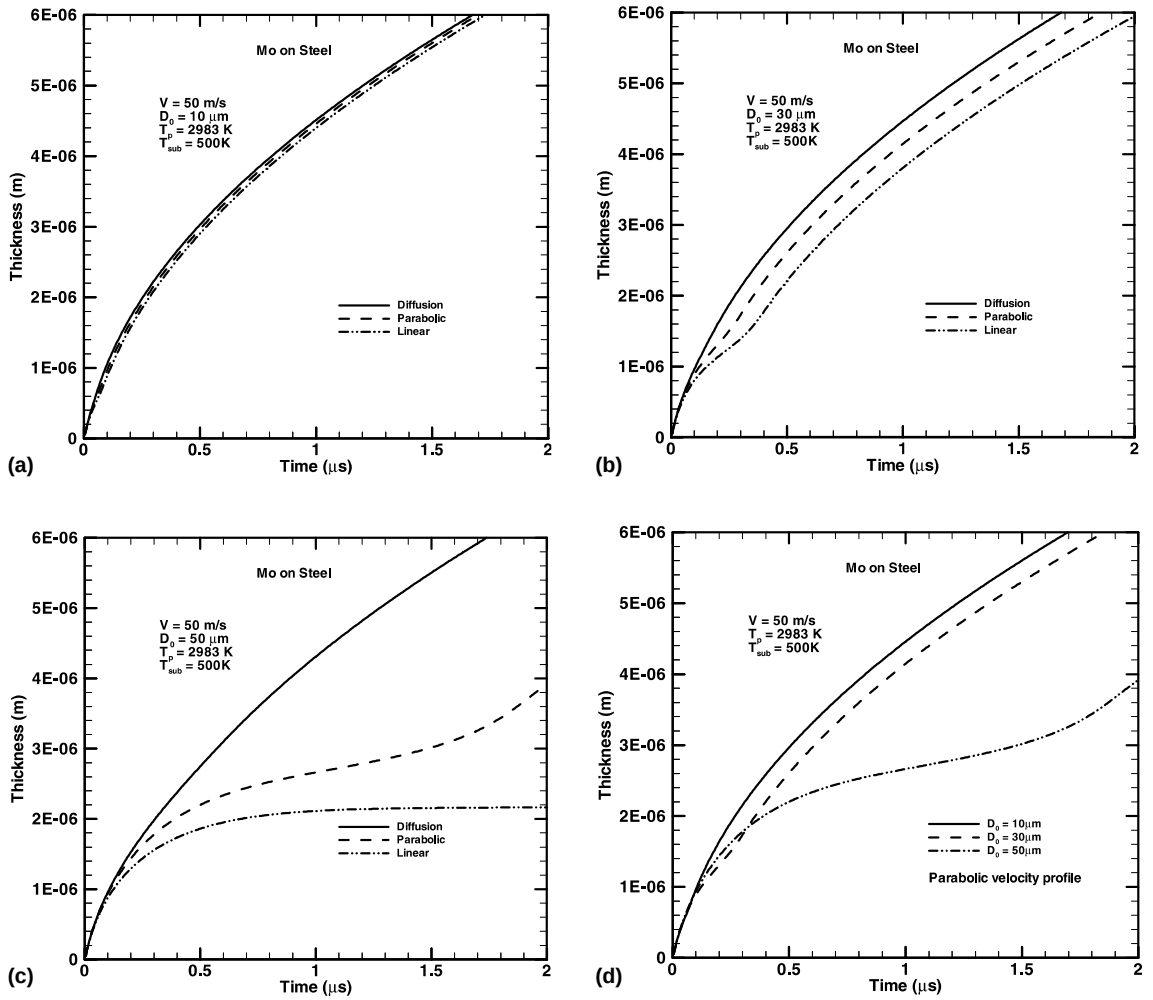

Fig. 4. The solidified thickness as a function of time for various initial droplet diameters ($D = 10, 30$, and 50 μm) under three different velocity profiles (diffusion, linear, and parabolic velocity profiles) during a molybdenum droplet impacting on a stainless steel substrate.

substrate surface. The effects of substrate temperature on the change of wetting ability are neglected in this study.

4.4. Effect of droplet temperature

A few studies [22,23] are conducted to investigate the effects of the initial droplet temperature on the solidification of superheated or supercooled molten metals on a substrate. Three droplet temperatures, 100 K superheated, melting temperature, and 100 K undercooled, are selected in this paper. Figs. 6(a)–(d) show the effects of melt flow on rapid solidification for different initial droplet temperatures using three velocity profiles (linear, parabolic, and diffusion). The solidification rate obtained from a higher initial droplet temperature is slightly slower than that from the diffusion case. For both linear and parabolic velocity profiles, the results are very different, especially for the linear case. It is not difficult to explain the phenomena since heat flux in the melt is proportional to the temperature difference between the melt and interface and heat transfer coefficient. The heat transfer coefficient is directly related to the velocity profile at the interface. For the diffusion case, heat transfer coefficient is at minimum. The effects of the initial droplet temperature on the solidification rate are therefore not significant for the diffusion model. The same conclusion has been drawn by others using one-dimensional rapid solidification models [22,23]. In reality, the effects may be very significant, as seen in Figs. 6(b) and (c). Fig. 6(d) demonstrates that the results from different profiles are virtually identical if initial droplet temperatures are equal to the equilibrium freezing temperature.

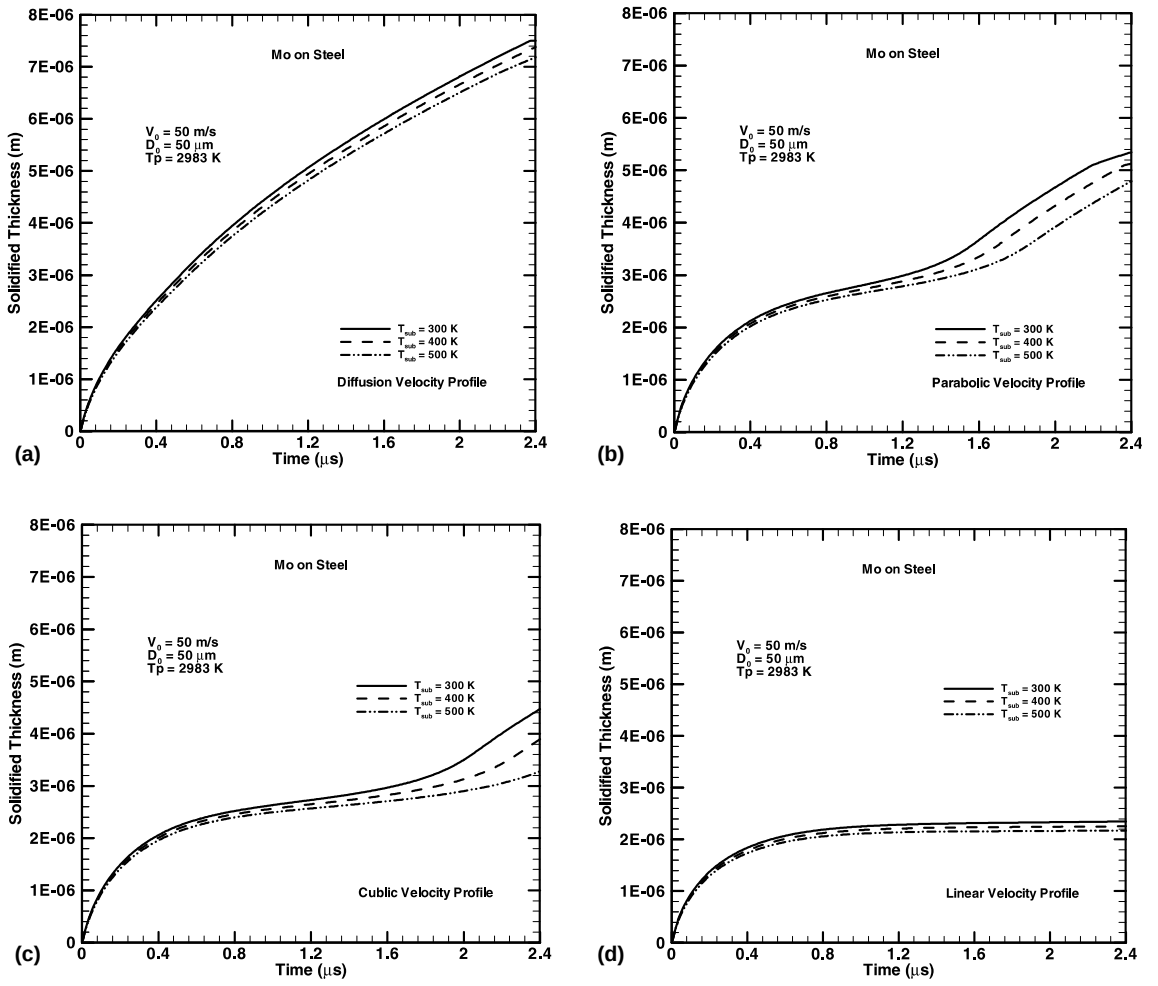

Fig. 5. The solidified thickness as a function of time for various initial substrate temperature ($T_{sub} = 300$, 400, and 500 K) under four different velocity profiles (diffusion, parabolic, cubic, and linear velocity profiles) during a molybdenum droplet impacting on a stainless steel substrate.

4.5. Effect of impinging velocity

To investigate the influence of impacting velocity on the solidification rate, the initial impinging velocities of 10, 30, and 50 m/s are chosen using three different velocity profiles (diffusion, linear, and parabolic). As shown in Fig. 7(a) and (b), the solidification rate decreases as the initial impact velocity increases from 10 to 50 m/s for the linear and parabolic velocity profiles. A larger solidification rate at a smaller impinging velocity is a result of the melt convection, which hinders droplet solidification. If the diffusion case is used, only one line is found (Fig. 7(c)). This indicates that the droplet impinging velocity has no influence on the solidification rate. Figs. 7(a) and (b) show the importance of melt flow on rapid solidification. For a smaller velocity of 10 m/s (see Fig. 7(d)), the solidification rates are almost the same for three velocity profiles. The melt flow becomes important when the impacting velocity reaches 30 m/s.

4.6. Effect of a pre-deposited splat

Experimental observation reveals that the pre-deposited splat significantly affects the morphology and solidification of the impinging droplet. The second droplet may splash since it interacts with the first pre-deposited droplet. The porosity formation of the coating might relate to the interaction. However, it is an extremely difficult task to consider it in a three-dimensional system together with rapid solidification (see Fig. 8). To simplify the problem, the interaction between the second droplet and a pre-deposited axisymmetric toroidal ring of molybdenum splat is investigated in this paper. The pre-deposited splat is obtained using the

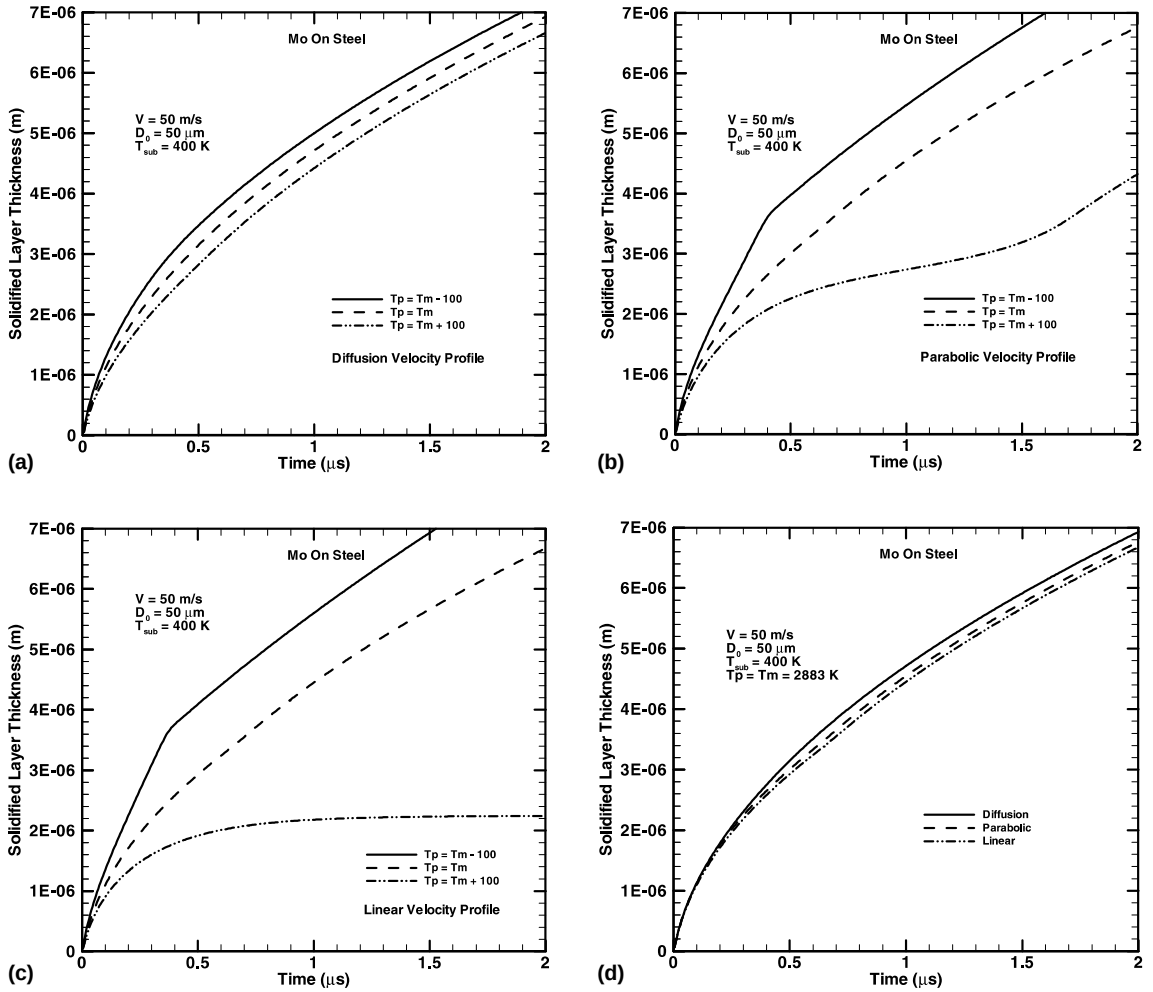

Fig. 6. The solidified thickness as a function of time for various initial droplet temperature ($T_p = T_m + 100$, T_m, and $T_m - 100$) under three different velocity profiles (diffusion, linear, and parabolic velocity profiles) during a molybdenum droplet impacting on a stainless steel substrate.

simulation result of a single droplet impacting on a steel substrate at 400 K. The shape of the first droplet is predicted and moved to a location away from the center. The cylindrical splat will then become an axisymmetric toroidal splat. To take into account of the total volume increase of the splat due to its movement, a smaller droplet is used to create the cylindrical splat whose size varies from 4.5 to 21 μm with an impinging velocity of 30 m/s, and a larger droplet is used as the impinging droplet, the second droplet, whose size varies from 15 to 70 μm. Fig. 9 shows the splat formation of a 15 μm diameter droplet with a velocity of 15 m/s impinging on a steel substrate. The melt flows over the pre-deposited splat without splashing. A deposited layer is built on the steel substrate and also pre-deposited splat. Rapid solidification is completed at about 3 μs. Fig. 10 shows the splashing pattern and splat formation of a larger impinging droplet interacting with the existence of the pre-deposited splat. Simulations have also been performed using the same conditions for a substrate without pre-deposited splat. A disk-like shape splat is predicted. It is evident that the splashing is due to the pre-deposited splat. Fig. 11 shows the pore formation for a droplet of 70 μm diameter with an impinging velocity of 10 m/s on a substrate with a pre-deposited splat. Due to the low velocity of the impinging droplet, the splashing behavior is limited. The melt is jetted away as a result of rapid solidification, and the jetted melt is re-attached to the substrate after a certain distance. A pore is formed due to the melt detachment at about 21 μs. The rough surface morphology of the deposited splat is due to low impinging velocity, high solidification rate and rough substrate. The results show that the model developed in this paper is capable of handling the influence of the

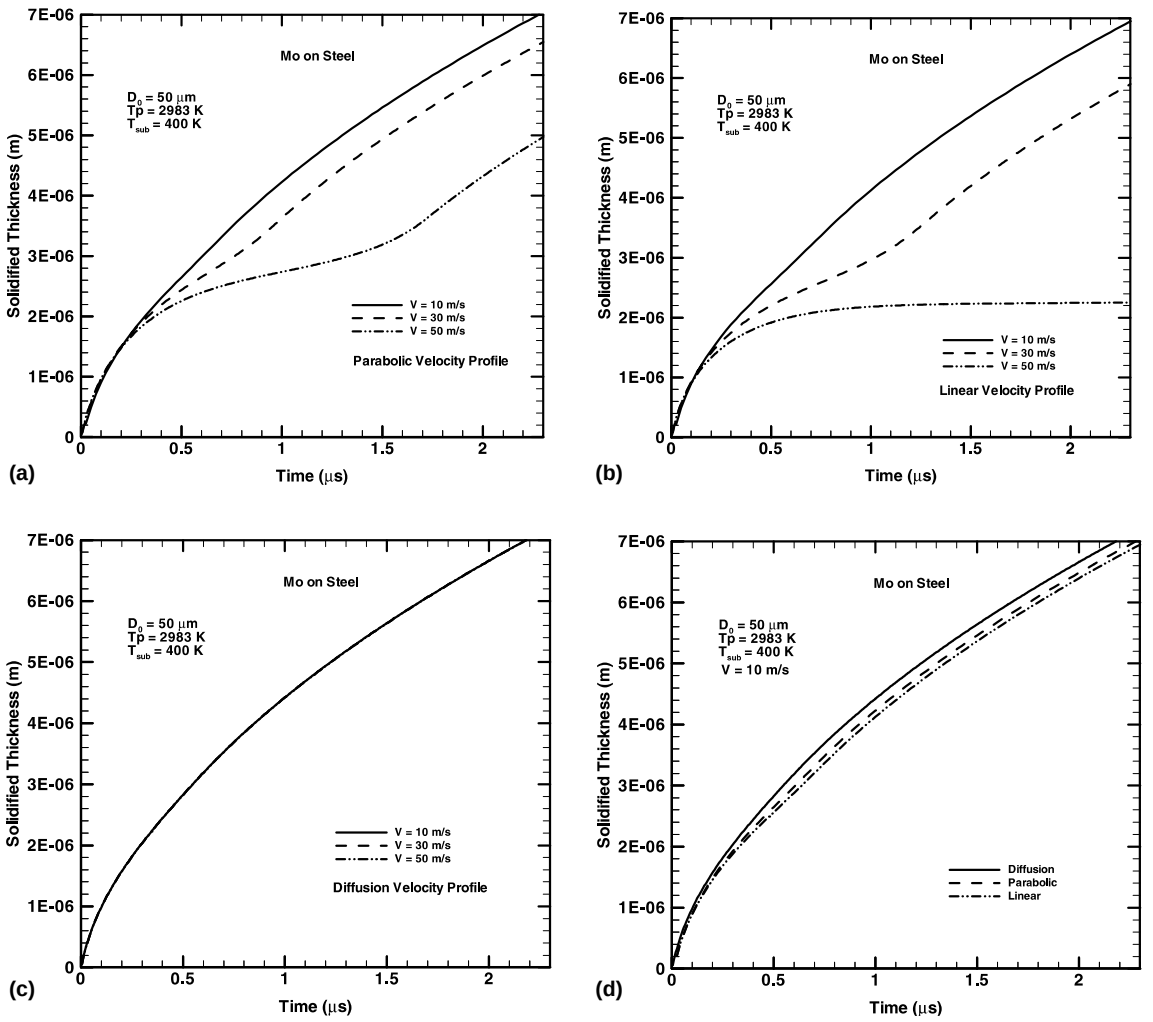

Fig. 7. The solidified thickness as a function of time for various initial droplet velocity $U = 10, 30$, and 50 m/s under three different velocity profiles (diffusion, linear, and parabolic velocity profiles) during a molybdenum droplet impacting on a stainless steel substrate.

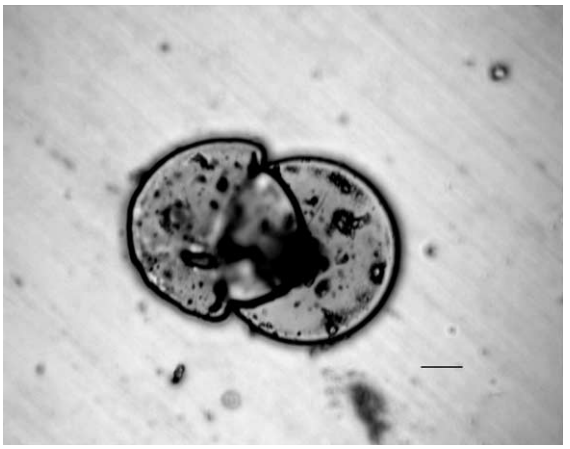

Fig. 8. Morphologies of two molybdenum splats on a steel substrate at 450 °C.

melt flow on rapid solidification for complicated processes.

5. Conclusions

A micro/macro-integrated model has been developed to simulation the evolution of droplet spreading and rapid solidification during thermal spray processes. The impact, spreading, and solidification of a molybdenum molten droplet impact on a stainless steel substrate have been investigated. Two levels of time-step and grid system have been used to combine a microscopic rapid solidification model and a macroscopic fluid flow model. The integration between the two models has been realized through a relational database in which several lookup tables were pre-created before simulations. The

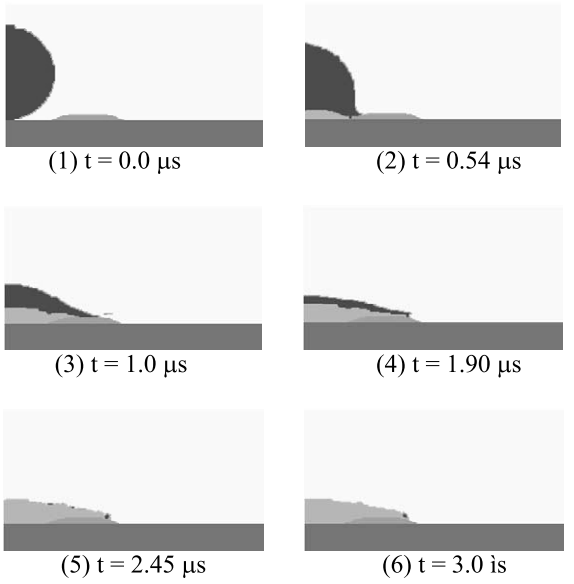

Fig. 9. Splat formation on a substrate with pre-deposited splat: sizes and velocities of the first and second droplets are $D_1 = 4.5$ μm, $V_1 = 30$ m/s, $D_2 = 15$ μm, and $V_2 = 15$ m/s, respectively.

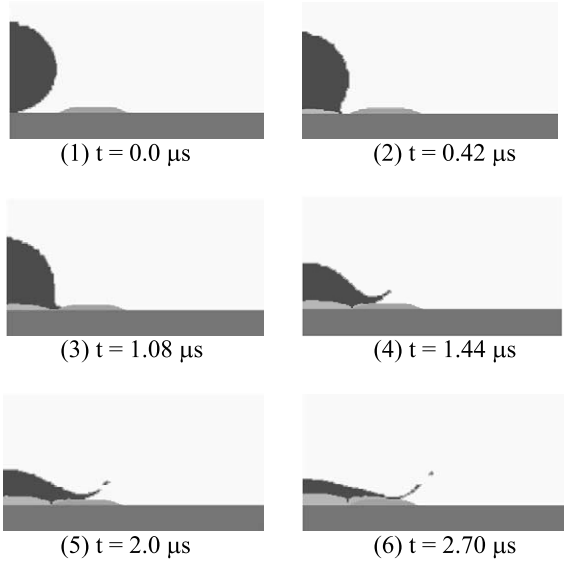

Fig. 10. Splat formation on a substrate with pre-deposited splat: sizes and velocities of the first and second droplets are $D_1 = 9$ μm, $V_1 = 30$ m/s, $D_2 = 30$ μm, and $V_2 = 15$ m/s, respectively.

effects of velocity profiles, droplet size, initial substrate temperature, initial droplet temperature, and initial impinging velocity on rapid solidification have been investigated. The results showed that melt flow plays a significant role on solidification, especially for a droplet

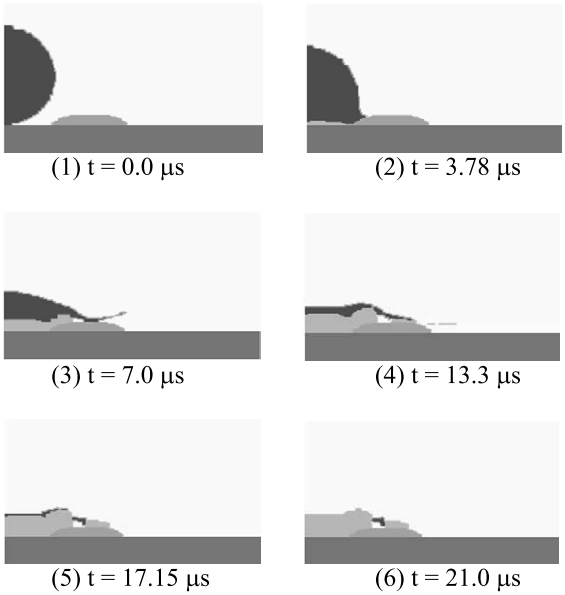

Fig. 11. Splat formation on a substrate with pre-deposited splat: sizes and velocities of the first and second droplets are $D_1 = 21$ μm, $V_1 = 30$ m/s, $D_2 = 70$ μm, and $V_2 = 10$ m/s, respectively.

size of greater 30 μm. It is crucial to consider the melt convection if the droplet is not at the equilibrium freezing temperature, and it is also important to choose a higher-order velocity profile. The initial droplet temperature and impinging velocity play significant roles in the droplet solidification. Effects of the pre-deposited splat on the morphology and solidification of the second droplet have been investigated for different sizes. No splashing has been observed for a smaller impinging droplet, whereas splashing occurs for a larger impinging droplet, and a pore may be formed for certain conditions.

Acknowledgements

This work was supported by the National Science Foundation under award No. CTS-9711135 and CTS-0074589 and MRSEC program under award No. DMR-9632570. Special thanks are due to Dr. H. G. Badr in computer science department at Stony Brook for helpful discussion in database communication between the micro- and macroscopic integration.

References

[1] D.B. Kothe, R.C. Mjolsness, M.D. Torrey, Ripple: a computer program for incompressible flows with free surfaces, Los Alamos National Laboratory Technical Report, LA-12007-MS, Los Alamos, New Mexico, 1991.

[2] G. Trapaga, J. Szekely, Mathematical modeling of the isothermal impingement of liquid droplets in spraying processes, Metall. Trans. 22B (1991) 901–914.
[3] G. Trapaga, E.F. Matthys, J.J. Valencia, J. Szekely, Fluid flow, heat transfer, and solidification of molten metal droplets impinging on substrates: comparison of numerical and experimental results, Metall. Trans. 23B (1992) 701–718.
[4] H. Liu, E.J. Lavernia, R.H. Rangel, Numerical simulation of impingement of molten Ti, Ni and W droplets on a flat substrate, J. Therm. Spray Technol. 2 (1993) 369–378.
[5] H. Liu, E.J. Lavernia, R.H. Rangel, Modeling of molten droplet impingement on a non-flat surface, Acta Metall. Mater. 43 (1995) 2053–2072.
[6] X. Bian, J.P. Delplanque, R.H. Rangel, Droplet deposition: comparison of models, numerical simulation and experimental results, in: Proc. 32nd Nat. Heat Transfer Conf., ASME, New York, NY, HTD, vol. 347, 1997, pp. 75–82.
[7] J. Fukai, Y. Shiiba, T. Yamamoto, O. Miyatake, D. Poulikakos, C.M. Megaridis, Z. Zhao, Wetting effects on the spreading of a liquid droplet colliding with a flat surface: experiment and modeling, Phys. Fluids 7 (1995) 236–247.
[8] Z. Zhao, D. Poulikakos, J. Fukai, Heat transfer and fluid dynamics during the collision of a liquid droplet on a substrate-I. modeling, Int. J. Heat Mass Transfer 39 (1996) 2771–2789.
[9] D. Poulikakos, J.M. Waldvogel, Heat transfer and fluid dynamics in the process of spray deposition, in: Advances in Heat Transfer, vol. 28, Academic Press, New York, NY, 1996, pp. 1–74.
[10] M. Pasandideh-Fard, J. Mostaghimi, On the spraying and solidification of molten particles in a plasma spray process: effect of thermal contact resistance, Plasma Chem. Plasma Process. 16 (1996) 83–S98.
[11] M. Pasandideh-Fard, R. Bhola, S. Chandra, J. Mostaghimi, Deposition of tin droplets on a steel plate: simulations and experiments, Int. J Heat Mass Transfer 41 (1998) 2929–2945.
[12] M. Chung, R.H. Rangel, Simulation of metal droplet deposition with solidification including undercooling and contact resystance effects, Numer. Heat Transfer A 37 (2000) 201–226.
[13] J.-P. Delplanque, R.H. Rangel, An improved model for droplet solidification on a flat surface, J. Mater. Sci. 32 (1997) 1519–1530.
[14] M. Pasandideh-Fard, J. Mostaghimi, S. Chandra, On a three-dimensional model of free surface flows with heat transfer and solidification, in: Proceedings of the 3rd ASME/JSME Joint Fluids Engineering Conference, FEDSM99-7112, San Francisco, 1999, pp. 1–6.
[15] L.L. Zheng, H. Zhang, An adaptive level set method for moving-boundary problems: application to droplet spreading and solidification, Numer. Heat Transfer B 37 (2000) 437–454.
[16] H. Zhang, X.Y. Wang, L.L. Zheng, X.Y. Jiang, Studies of splat morphology and rapid solidification during thermal spraying, Int. J Heat Mass Transfer 44 (2001) 4579–4592.
[17] C.H. Amon, K.S. Schwaltz, R. Merz, F.B. Prinz, Numerical and experimental investigation of interface bonding via substrate remelting of an impinging molten metal droplet, J. Heat Transfer 118 (1996) 164–172.
[18] G.X. Wang, E.F. Matthys, Experimental investigation of interfacial thermal conductance for molten metal solidification on a substrate, J. Heat Transfer 118 (1996) 157–163.
[19] S.P. Wang, G.X. Wang, E.F. Matthys, Deposition of a molten layer of high melting point material: substrate melting and resolidification, Mater. Sci. Eng. A 262 (1999) 25–32.
[20] H. Zhang, Theoretical analysis of spreading and solidification of molten droplet during thermal spray deposition, Int. J. Heat Mass Transfer 42 (1999) 2499–2508.
[21] J. Madejski, Solidification of droplets on a cold surface, Int. J. Heat Mass Transfer 19 (1976) 1009–1013.
[22] G.X. Wang, E.F. Matthys, Heat transfer modeling of rapid solidification on a substrate: a parametric investigation for large undercooling, Int. J. Rapid Solidificat. 6 (1991) 297–324.
[23] T.W. Clyne, Numerical treatment of rapid solidification, Met. Trans. B 15 (1984) 369–381.